Neuron
Article

Establishment of Neurovascular Congruency in the Mouse Whisker System by an Independent Patterning Mechanism

Won-Jong Oh[1] and Chenghua Gu[1,*]
[1]Department of Neurobiology, Harvard Medical School, 220 Longwood Avenue, Boston, MA 02115, USA
*Correspondence: chenghua_gu@hms.harvard.edu
http://dx.doi.org/10.1016/j.neuron.2013.09.005

SUMMARY

Nerves and vessels often run parallel to one another, a phenomenon that reflects their functional interdependency. Previous studies have suggested that neurovascular congruency in planar tissues such as skin is established through a "one-patterns-the-other" model, in which either the nervous system or the vascular system precedes developmentally and then instructs the other system to form using its established architecture as a template. Here, we find that, in tissues with complex three-dimensional structures such as the mouse whisker system, neurovascular congruency does not follow the previous model but rather is established via a mechanism in which nerves and vessels are patterned independently. Given the diversity of neurovascular structures in different tissues, guidance signals emanating from a central organizer in the specific target tissue may act as an important mechanism to establish neurovascular congruency patterns that facilitate unique target tissue function.

INTRODUCTION

The nervous and vascular systems are highly branched networks that are functionally and physically interdependent (Carmeliet and Tessier-Lavigne, 2005; Zlokovic, 2008). Blood vessels provide neurons with oxygen and nutrients and protect them from toxins and pathogens. Nerves, in turn, control blood vessel diameter and other hemodynamic parameters such as heart rate. The functional interdependence between nerves and vessels is reflected in their close anatomic apposition. In the periphery, nerves and vessels often run parallel to one another, a phenomenon called neurovascular congruency (Bates et al., 2003; Quaegebeur et al., 2011). The intimate association between neurons and vessels is particularly important in the brain, as neural activity and vascular dynamics are tightly coupled by a neurovascular unit (Iadecola, 2004). Moreover, recent evidence suggests that some neurodegenerative diseases once thought to be caused by intrinsic neuronal defects are initiated and perpetuated by vascular abnormalities (Quaegebeur et al., 2011; Zlokovic, 2011). Despite these important connections between the nervous and vascular systems, a key unsolved question is how nerves and vessels become physically aligned during development in order to facilitate their functional properties.

The similar branching pattern of nerves and blood vessels was first noted in the scientific literature over 100 years ago (Lewis, 1902). Since then, tightly associated nerves and blood vessels have been termed "neurovascular bundles," and the phenomenon itself has been named "neurovascular congruency" (Martin and Lewis, 1989; Taylor et al., 1994). While the existence of neurovascular bundles is widespread, the best studied example is the vertebrate forelimb skin, where congruency has been shown to be established during embryogenesis. Arteries are aligned with peripheral nerves in embryonic mouse limb skin, and in mice with mutations that lead to disorganized nerves, blood vessels follow these misrouted axons. Therefore, in the developing mouse forelimb skin system, peripheral sensory nerves determine the differentiation and branching pattern of arteries (Mukouyama et al., 2002, 2005), indicating that the nerve guides the vessel. Mukouyama et al.'s elegant study suggests that neurovascular congruency can be established by a general principle of "one-patterns-the-other," in which either the nervous or vascular system precedes in development and then instructs the second system to form using the already established architecture as a template. However, this particular example describes the relatively simple planar structure of skin, and, given the diversity of neurovascular networks in different tissues, the "one-patterns-the-other" model is perhaps not precise enough to serve as a general mechanism governing the establishment of neurovascular congruency in all tissues, especially where more complex neurovascular associations and spatially restricted three-dimensional (3D) structures exist.

The whisker pad system provides an excellent model to study how neurovascular congruency arises in target tissues with complex, 3D anatomy. Whiskers are patterned in discrete arrays with invariant numbers in each row of follicles. The whisker pad that underlies each individual whisker receives primary somatosensory innervation from axons in the maxillary branch of the trigeminal nerve and then faithfully relays the sensory information to the brain (Erzurumlu et al., 2010). In the mature whisker pad, each whisker is innervated by multiple types of trigeminal neurons that form morphologically distinct endings inside the follicular sinus complex (FSC) (Ebara et al., 2002). Similarly, each whisker is inhabited by a branch of the

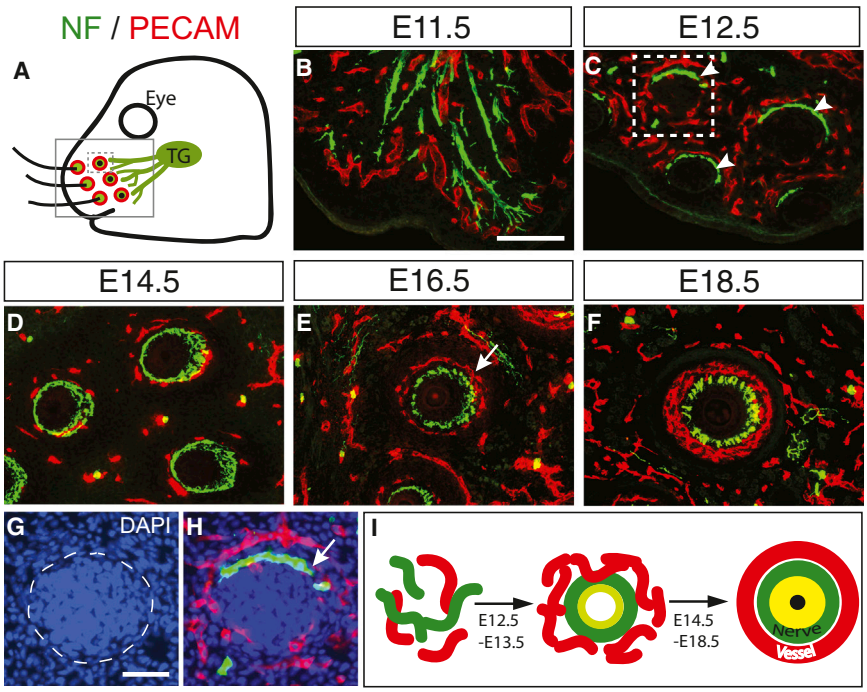

Figure 1. Nerve and Blood Vessels Are Organized into a Double Ring Structure in the Whisker Follicle during Development

(A–F) Developmental profile of trigeminal axon innervation and blood vessel patterning in the whisker follicles. Trigeminal axons and blood vessels are visualized by neurofilament (NF; green) and PECAM (red), respectively, in the snout area, indicated by boxed region in (A). Coimmunostained tangential sections of whisker follicles at E11.5 (B), E12.5 (C), E14.5 (D), E16.5 (E), and E18.5 (F) show the dynamic processes that lead to the stereotypic organization of a double ring structure. The trigeminal axons form a ring-like structure as early as E12.5, indicated by arrowheads in (C), and are then surrounded by a blood vessel ring that results in the formation of a double ring structure around each follicle at E16.5, with the nerve ring located inside and the vessel ring outside, indicated by an arrow in (E). Scale bar in (B), 100 μm, also applies to (C) through (F).

(G and H) One whisker follicle, indicated by the dotted box in (C), is overlaid by DAPI staining to show follicle primordium, indicated by the dotted circle in (G). Nerve terminals surround the outside of the primordium, indicated by the arrow in (H). Scale bar in (G), 50 μm.

(I) Schematic illustration of nerve and vessel ring organization in the whisker follicle.

See also Figure S1 and Movies S1, S2, and S3.

infraorbital artery, which establishes the intricate capillary network called the blood sinus surrounding the follicle and forms the FSC (Ebara et al., 2002; Katsume et al., 1984; Fundin et al., 1997). Therefore, in the adult, each follicle is surrounded by a well-organized layer of nerve endings and an adjacent vascular network. The vascular component affiliated with each whisker affects the movement of the whisker (Wineski, 1985) and modulates the sensitivity of the sensory nerve endings (Fundin et al., 1997; Wineski, 1985). Thus, neurovascular organization in each follicle is critical for precise whisker function.

In this study, we found that the close association between sensory nerves and blood vessels in the whisker pad is established during development. We observed a dynamic nerve/vessel interaction that ultimately results in the stereotypic organization of a "double ring" structure around each follicle. Surprisingly, nerve and vessel rings form independently rather than through a "one-patterns-the-other" model. We further demonstrate, through the use of mouse genetics, that secreted Semaphorin 3E and its receptor Plexin-D1 signaling is required to establish a stereotypic double ring neurovascular structure around each whisker follicle. Sema3E has the potential to repel both nerves and vessels through Plexin-D1. Sema3E originating from the follicle controls the organization of the outer vessel ring while the selective downregulation of Plexin-D1 permits the nerves to maintain their inner ring position. Given the broad diversity of neurovascular structures and the need for individualized function, the copatterning/independent-patterning mechanism by guidance signals emanating from a central organizer in the specific target tissue is likely to be a common mechanism that is used to establish neurovascular congruency patterns in complex tissues.

RESULTS

Nerves and Vessels Form a Stereotypic Double Ring Structure around Each Whisker Follicle, with the Nerve Ring Inside and the Vessel Ring Outside

To characterize how follicular neurovascular organization arises during development, we performed double immunostaining to detect axons (antineurofilament; green) and blood vessels (anti-PECAM; red) during different developmental stages. We found that trigeminal axons arrive at the whisker primordium as early as embryonic day (E)10.5, as was previously reported (Stainier and Gilbert, 1990). The primary vascular plexus is already formed at this time and is intermingled with the incoming axons until E11.5 (Figure 1B). Around E12.5, a ring-like structure of axonal innervation forms around each whisker primordium, while vessels remain disorganized and partially intermingled with the axons (Figures 1C, 1G, and 1H; Figure S1A available online; Movie S1). By E14.5, vessels are recruited to the nerve ring, leading to close apposition of vessels and axons (Figures 1D and S1B; Movie S2). By E16.5, a prominent double ring structure is formed, with a ring of nerves on the inside, a ring of vessels on the outside, and a defined space between them (Figures 1E and S1C; Movie S3). At E18.5, both nerve and vessel ring patterning are further refined (Figure 1F). The nerve-inside and vessel-outside structure is maintained during adulthood and is known to be important for whisker function (Ebara et al., 2002). This relatively simple system with clear stereotypic developmental characteristics (Figure 1I) allows us to dissect the molecular and cellular interactions between nerves and vessels in a systematic, stepwise manner.

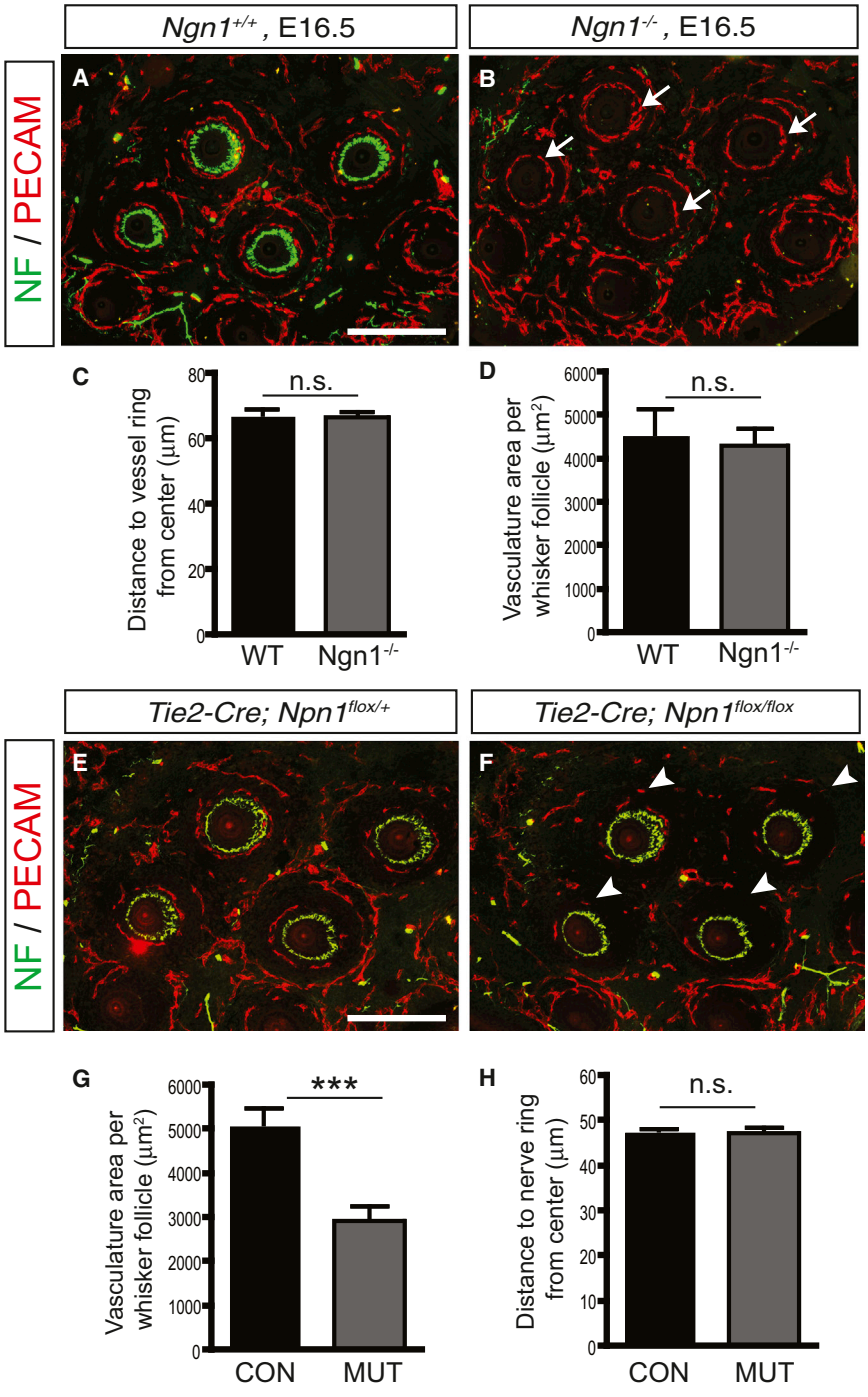

Figure 2. Nerve Ring and Vessel Ring Are Patterned Independently of Each Other in the Whisker Follicle

(A–D) Nerve/vessel immunostaining of wild-type littermate control exhibits normal double ring patterning (A). Nerve/vessel immunostaining of the *Ngn1* knockout shows no trigeminal innervation in the whisker follicles, but blood vessel rings are normally organized at each whisker follicle, indicated by arrows in (B), (C), and (D). For the quantification, ten pairs of whisker follicles were analyzed, and the mean distance from the center (C) and vasculature area surrounding the follicle (D) ±SEM are shown. NF, neurofilament.

(E–H) Endothelial specific-*Npn1* deletion shows less vasculature formation around whisker follicle, shown by white arrowheads in (F) and (G), compared to the vasculature of control (E), but nerve rings are organized normally (H). Vasculature area surrounding follicle (G) and mean distance from center to nerve ring (H) ±SEM are also shown (n = 14). Paired Student's t test; ***p < 0.001; n.s, not significant.

Scale bars, 200 μm.

Nerve Ring and Vessel Ring Are Patterned Independently of Each Other in the Whisker Follicles

Based on the developmental profile of nerve and vessel organization in the whisker follicle, the "one-patterns-the-other" model of neurovascular congruency would predict that the trigeminal axons attract surrounding blood vessels to establish the double ring structure. To examine this possibility, we analyzed the nerve/vessel organization in the whisker follicle of neurogenin-1 (Ngn1) knockout embryos, in which trigeminal ganglia (TG) and thus the trigeminal nerves are completely absent (Ma et al., 1998). To our surprise, vessel ring organization is completely normal in *Ngn1* knockouts at E16.5 (Figure 2B), despite the lack of nerve ring formation (absence of green signal in Figure 2B). Both the size and position of the vessel ring in *Ngn1* mutant and wild-type littermate controls has no detectable difference (Figures 2C and 2D). This result clearly demonstrates that unlike limb skin (Mukouyama et al., 2002), where arterial patterning is disrupted in *Ngn1/2* knockouts, indicating that sensory axons determine the patterning of arteries, here the formation of the vascular ring structure is independent of the nerves.

Next, we examined whether blood vessel ring patterning has any effect on nerve ring formation. We analyzed the double ring structure in endothelial-specific neuropilin-1 (Npn-1) null mice (*Tie-2 Cre; Npn1* $^{flox/flox}$) where the vasculature surrounding the whisker follicles is poorly developed (Figures 2E and 2F) (Gu et al., 2003). However, nerve ring formation shows no detectable difference between mutants and control littermates (Figures 2G and 2H). This result demonstrates that nerve ring formation is also independent of vessel ring formation. Therefore, the neurovascular congruency of the double ring pattern in the whisker follicles is not established by the "one-patterns-the-other" mechanism, but rather patterned independently.

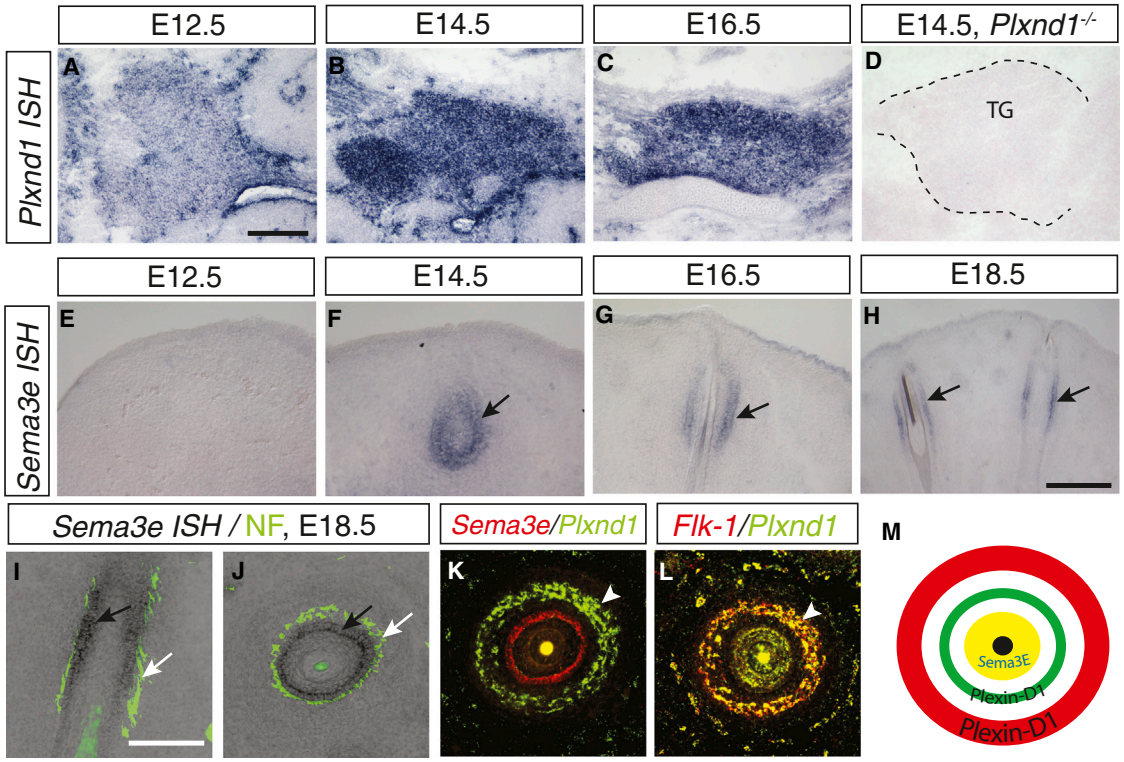

Figure 3. Complementary Expression Pattern of Plexin-D1 in the TG and Blood Vessels and Sema3E in the Whisker Follicle

(A–D) *Plxnd1* ISH on sagittal sections of wild-type embryos at E12.5 (A), E14.5 (B), and E16.5 (C) shows that *Plxnd1* mRNA is detected at very low levels as early as E12.5 and is significantly increased at E14.5 and continues on to E16.5 as the double ring structure develops. *Plxnd1* mRNA is not detectable in sections of the TG from plexin-D1 knockout animals at E14.5. TG is outlined by the dashed line in (D). Scale bar in (A), 100 μm.

(E–H) *Sema3e* mRNA ISH on coronal sections parallel to the whisker follicles at E12.5 (E), E14.5 (F), E16.5 (G), and E18.5 (H) shows that *Sema3e* mRNA is expressed in the mesenchymal sheath surrounding the hair follicles starting at E14.5 and continues at E16.5 and E18.5 (black arrows). Scale bar in (A), 100 μm, also applies to (G); scale bar in (H), 200 μm.

(I and J) Neurofilament (NF) immunostaining (white arrows) after *Sema3e* ISH on the same sections shows that *Sema3e* (black arrows) is expressed inside of the nerve rings, indicated by the coronal image in (I) and the tangential image in (J). Scale bar in (I), 100 μm.

(K and L) Double fluorescence ISH with *Plxnd1* and *Sema3e* (K) or *Flk-1* (L) shows that *Plxnd1* mRNA is expressed in the endothelial cells that form the vessel ring, indicated by a white arrowhead in (K) and (L), and *Sema3e* is expressed inside of both nerve and vessel rings. Scale bar in (I), 100 μm, also applies to (L).

(M) Summary of *Plxnd1* and *Sema3e* mRNA expression pattern in the whisker follicle. *Sema3e* is expressed in mesenchymal tissue (yellow), and *Plxnd1* is expressed in blood vessel (red) and in TG therefore Plexin-D1 protein probably in nerve (green).

Sema3e and *Plxnd1* Are Complementarily Expressed in the Trigeminal-Whisker Follicle System

To reveal the mechanism governing the neurovascular congruency in the whisker pad system, we first considered the contributions from the target tissues on their coordinated patterning. Emerging evidence suggests that the neural and vascular systems share many similar mechanisms and molecular cues to regulate their development (Adams and Eichmann, 2010; Carmeliet and Tessier-Lavigne, 2005; Gelfand et al., 2009). Therefore, we next asked whether guidance cues could be found in the whisker follicle, and whether these cues could function as an organizing signal to coordinately pattern the nerves and vessels into the congruent double ring structure. We first performed expression screening of known guidance molecules in the TG and whisker targets, and found a striking complementary expression pattern of *Sema3e* and its receptor *Plxnd1* in these areas (Figures 3A–3H). Moreover, the spatiotemporal expression of these molecules coincides with the developmental profile of whisker follicles. *Plxnd1* mRNA was expressed at very low levels in the TG neurons at an early stage (E12.5), when axons arrive at the whisker target (Figure 3A) (van der Zwaag et al., 2002). Its expression level is significantly increased by E14.5, when trigeminal axons and blood vessels begin to organize the double ring structure in the whisker follicles (Figure 3B) and continues through E16.5 and E18.5, when target innervation is refined and a clear double ring structure is apparent (Figure 3C; data not shown). In a manner similar to the temporal profile of *Plxnd1* expression in the TG, *Sema3e* is not expressed at E12.5 in the whisker follicles (Figure 3E). *Sema3e* mRNA is found in the mesenchymal sheath surrounding the hair follicles starting at E14.5 and continuing to E16.5 and E18.5 (Figures 3F–3H). To characterize the precise location of *Sema3e* within the follicle, we performed immunostaining of axons after *Sema3e* in situ hybridization (ISH) on the same tissue sections and demonstrated that *Sema3e* was expressed inside the nerve ring (Figures 3I and 3J). Finally, to examine whether *Plxnd1* is also expressed in the

outer blood vessel ring, we performed double fluorescence ISH of *Plxnd1* and the endothelial cell marker *Flk-1*. As shown in Figure 3L, mRNA expression of *Plxnd1* and *Flk-1* completely overlaps within the vessel ring. Together, these expression data suggest that, in the whisker pad, Sema3E expression surrounds the hair follicle (Figures 3K and 3M), while Plexin-D1 is expressed in the blood vessels and may also expressed in the innervating trigeminal axons based on its mRNA expression in the TG (Figure 3M). This complementary expression pattern in the target area suggests that Sema3E-Plexin-D1 signaling plays a role in coordinating trigeminal target innervation and the formation of blood vessels into the double ring structure.

Semaphorin 3E and Its Receptor Plexin-D1 Facilitate Repulsive Signaling in Both Nerves and Vessels

Does Sema3E function as a common cue to coordinately pattern nerves and vessels during the formation of the stereotypic double ring structure? Because trigeminal axon terminals in the whisker target are adjacent to *Sema3e*-expressing cells (Figures 3I and 3J), whereas blood vessels are located outside of the nerve ring (Figures 3K and 3L), we first tested the hypothesis that Sema3E may act as an attractive cue to trigeminal axons and a repulsive cue to blood vessels. Such an attractive guidance role for axons is consistent with the prior observation that, in the presence of neuropilin-1, a coreceptor for Plexin-D1, Sema3E can serve as an attractant (Chauvet et al., 2007), and it is consistent with our observation that Npn-1 is highly expressed in the TG at this stage (Figure S2B). However, to our surprise, application of alkaline phosphatase (AP)-tagged Sema3E to E14.5 TG explants induced significant growth cone collapse (Figure 4C) compared to the control AP-treated group (Figure 4A). Moreover, Sema3E-induced growth cone collapse was absent in trigeminal neurons isolated from *Plxnd1* null mice (Figure 4D), indicating that Sema3E serves as a repulsive cue to trigeminal neurons and that Plexin-D1 is required for its effects. To further examine whether Npn-1 plays any role in Sema3E-induced trigeminal growth cone collapse, we performed the same growth cone collapse assay using TG explants from Nestin-Cre-driven *Npn1* conditional knockout embryos in which Npn-1 was ablated in all neuronal populations. TG isolated from these mice exhibit the same level of growth cone collapse as their wild-type littermate controls when treated with AP-Sema3E (Figures S2E and S2F), indicating that Sema3E-Plexin-D1 signaling induces trigeminal growth cone collapse independent of Npn-1. As a positive control, we also treated TG explants from these mice with AP-Sema3A. Sema3A-Npn-1 signaling causes trigeminal growth cone collapse in vitro and is required for the initial axon projection from the TG to their peripheral targets in vivo (Gu et al., 2003; Kobayashi et al., 1997)(Figures 4E and 4F). As expected, axons from TG isolated from *Nestin-Cre; Npn1*$^{flox/flox}$ mice were completely unresponsive to the Sema3A-induced growth cone collapse (Figure S2H). Finally, although vascular endothelial growth factor receptor 2 (VEGFR2/Flk-1) has been suggested to promote axonal growth in association with Plexin-D1/Neuroplin-1 receptor complex (Bellon et al., 2010), VEGFR2 is not expressed in the TG neurons during double ring formation (Figure S2K). Therefore, Sema3E acts on trigeminal axons as a repellant rather than an attractant.

To examine the effect of Sema3E on endothelial cells, we performed an in vitro transwell migration assay using human umbilical vein endothelial cells (HUVECs), which endogenously express Plexin-D1. As predicted, vascular endothelial growth factor (VEGF) caused the majority of endothelial cells to migrate to the bottom chamber (Figures 4J and 4L), reflecting the known function of VEGF as an attractant for these cells. However, when Sema3E and VEGF were added together, almost no migration was observed (Figures 4K and 4L), indicating that Sema3E inhibits VEGF-induced migration. Moreover, Sema3E also blocked the basal level of migration (Figure 4I). Together, these results support the idea that Sema3E can dominantly block the attractive effects exerted upon Plexin-D1-expressing endothelial cells.

Differential Expression of Plexin-D1 Protein Allows for Distinctive Responses of Nerves and Vessels to Sema3E

The appealing hypothesis that emerged, based on these in vitro results, is that Sema3E acts as a repulsive guidance cue for both trigeminal axons and blood vessels and serves to organize the double ring neurovascular structure surrounding the follicle. If this hypothesis is true, what accounts for the relative position of the nerves and vessels, with the nerve ring consistently positioned inside of the vessel ring? In particular, it is puzzling how trigeminal axons expressing Plexin-D1 are able to innervate an area that is so close to a secreted repulsive cue. One potential possibility is that the abundance of *Plxnd1* mRNA transcripts in the TG may not reflect protein levels at the nerve terminal. To test this idea, we performed AP-Sema3E binding on tissue sections to detect Plexin-D1 protein along the trigeminal nerve (Chauvet et al., 2007; Gu et al., 2005). As shown in Figure 5A, although Plexin-D1 protein is highly expressed in the trigeminal nerves projecting to the whisker follicle, surprisingly, Plexin-D1 protein is very low in the nerve terminals (white arrowheads in Figures 5B and 5C). This difference is not due to our inability to detect protein binding at the nerve terminal, because Npn-1 protein is equally well detected in both the projecting axons and the nerve terminal by AP-Sema3A binding (arrowheads in Figures 5D and 5E). The absence of AP-Sema3E binding on the vessel ring (red arrow in Figure S3C) of *Plxnd1* null mice further confirmed that Plexin-D1 is the only receptor for Sema3E in the vessel ring (Figures S3A–S3D). The absence of AP-Sema3E binding on the nerve ring in *Sema3e* null mice also ruled out the possibility that the lack of AP-Sema3E binding may be due to the sequestration of Plexin-D1 by endogenous Sema3E (Figures S3E–S3H). To further confirm the selective downregulation of Plexin-D1 protein in the TG nerve terminals, we also performed anti-Plexin-D1 immunohistochemistry (Chauvet et al., 2007). Consistent with the AP-Sema3E binding result, TG nerve terminal exhibited extremely low Plexin-D1 immunoreactivity (Figures 5F and 5G). Therefore, the Plexin-D1 protein is selectively downregulated in the TG nerve terminals, which enables the nerves to innervate areas close to the Sema3E-expressing region and form the inner ring. In stark contrast to the low expression of Plexin-D1 in the nerve ring, the Plexin-D1 protein level visualized by both AP-Sema3E and anti-Plexin-D1 antibodies in the blood vessels is remarkably high (white arrows in Figures 5B, 5C, 5H, and 5I). Therefore, the differential expression of localized Plexin-D1 protein may lead to a differential response between the nerves and

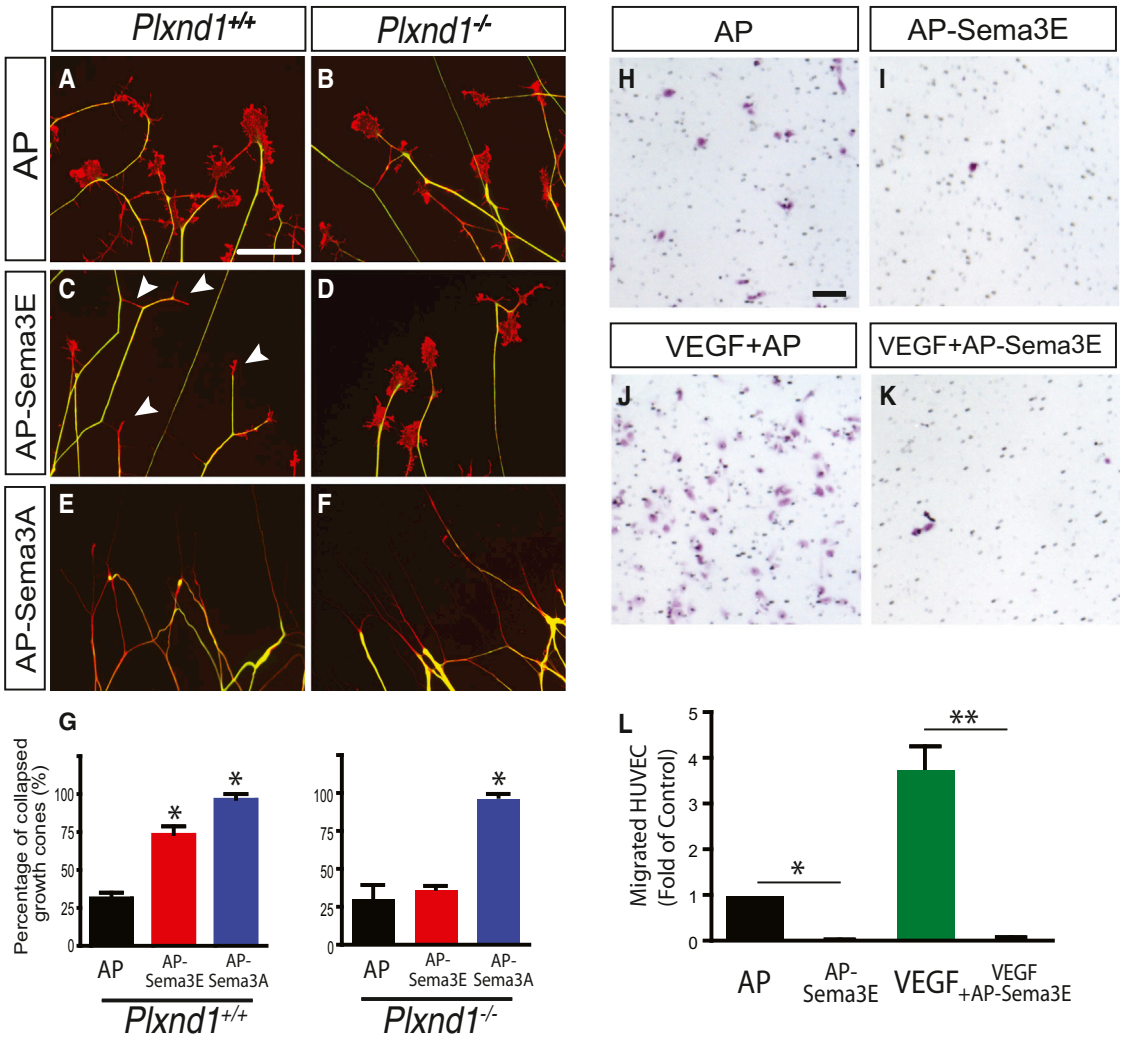

Figure 4. Sema3E-Plexin-D1 Signaling Provides a Repulsive Guidance Cue to Both TG Axons and Blood Vessels In Vitro

(A–G) Sema3E-Plexin-D1 signaling serves as repulsive cue for cultured TG neurons. TG were isolated from wild-type in (A), (C), and (E) or *Plxnd1* null mice in (B), (D), and (F) at E14.5, and a growth cone collapse assay was performed. Axons (green) and growth cones (red) were visualized by antineurofilament and phalloidin staining, respectively. After incubation with 2 nM of AP, shown in (A) and (B); AP-Sema3E, shown in (C) and (D); or AP-Sema3A, shown in (E) and (F) for 30 min, >200 growth cones were scored for each experimental condition. Sema3E treatment induced significant growth cone collapse, indicated by white arrowheads in (C), but growth cone collapse was absent in *Plxnd1* mutant TG neurons (D). (G) shows quantification of growth cone collapse assay (n = 3; data shown as mean ± SD, ANOVA; *p < 0.001). Scale bar in (A), 50 μm, also applies to (B) through (F).

(H–L) Sema3E inhibits endothelial cell migration. VEGF-induced HUVEC transwell migration assay was performed in the presence (K) or absence (J) of Sema3E (AP-Sema3E, 0.5 nM). After a 5 hr incubation, migrated cells were fixed and visualized by Nissl staining. Sema3E prevents HUVEC migration induced by VEGF as well as the basal level of migration (I). (L) Quantification of migrated HUVECs (data shown as mean ± SEM, n = 3, ANOVA; *p < 0.05; **p < 0.001). Scale bar in (H), 50 μm, also applies to (I) through (K).

See also Figure S2.

vessels to Sema3E, resulting in the nerve-inside and vessel-outside double ring structure.

Sema3E-Plexin-D1 Signaling Is Required for Proper Double Ring Formation In Vivo

To directly test the in vivo requirement of Sema3E-Plexin-D1 signaling in the formation of the neurovascular double ring structure in each whisker follicle, we analyzed nerve and vessel patterning in the developing whisker follicle in *Plxnd1* null and *Sema3e* null embryos. In wild-type embryos at E16.5, the outer ring of blood vessels is distinctly separated from the inner ring of nerves (Figures 6A and 6D). However, in the mutant embryos, the two rings are intermingled (arrows in Figures 6B and 6E). To quantitatively analyze this phenotype, we measured the ratio between the inner ring radius, r, and outer ring radius, R, in the same follicle and then compared the averaged ratios from wild-type embryos to that in mutant mice (Figure 6I). We observed a significant increase in the r/R ratio in the mutant

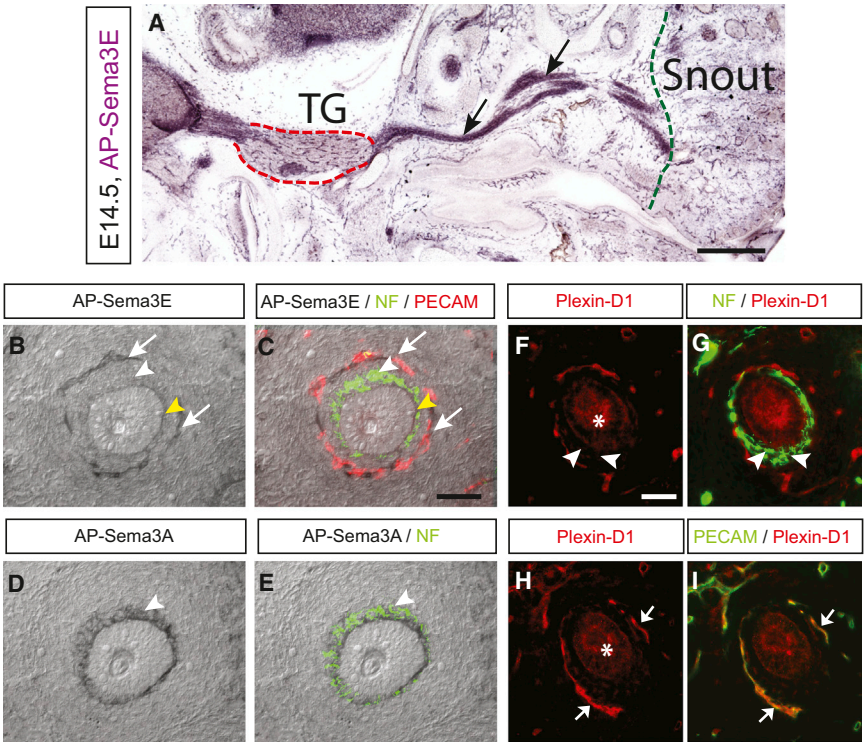

Figure 5. Plexin-D1 Protein Expression Is Selectively Downregulated in the Target Terminal of TG Axons

(A–C) Plexin-D1 protein expression is visualized by AP-Sema3E binding. Tangential sections of tissue were cut at E14.5 and then incubated with 1 nM AP-Sema3E. Binding was then detected by reaction with an AP substrate. Plexin-D1, indicated by black arrows in (A), is highly expressed within the TG (dotted red outline) and the trigeminal nerves that project both centrally toward the brain stem and peripherally toward the snout (right side from dotted green outline). However, Plexin-D1 protein is extremely low in nerves when they reach the whisker follicle, as indicated by the white arrowheads in (B) and (C). In contrast, Plexin-D1 protein is strongly detected in the blood vessel ring, indicated by white arrows in (B) and (C). Yellow arrowheads in (B) and (C) indicate nonspecific signals in the membrane structure of the whisker follicle. In (C), to identify the relative location of nerve and blood vessel rings, adjacent sections were immunostained with neurofilament (NF; green) and PECAM (red) and overlaid on to the AP-stained sections. Scale bar in (A), 1 mm; scale bar in (C), 50 μm.

(D and E) Neuropilin-1 protein expression is detected by AP-Sema3A (2 nM) binding in the terminal nerve ring, indicated by arrowheads in (D) and (E), which completely overlaps with the NF-positive nerve ring on the same sections after AP staining (E).

(F–I) Plexin-D1 protein expression is visualized by immunohistochemistry with anti-Plexin-D1. In the TG nerve terminal surrounding the whisker follicles, Plexin-D1 protein expression is extremely low, indicated by arrowheads in (F) and (G). In contrast, Plexin-D1 protein is strongly detected in the blood vessel ring, indicated by arrows in (H) and (I). Anti-Plexin-D1 displays nonspecific signals in the hair sheath and glassy membrane of the whisker follicle, indicated by asterisks in (F) and (H). Scale bar in (F), 50 μm.

See also Figure S3.

animals as compared to the wild-type littermate controls, reflecting a collapsed double ring structure in the mutant mice (Figures 6C and 6F). The average distances from the follicle center to nerve/vessel ring in mutants and controls were also measured, respectively (Figures S4A and S4B). The vessel ring moved inward significantly, whereas nerve ring position relative to center showed no noticeable changes, consistent with the selective downregulation of Plexin-D1 at the nerve terminal. To see clear structure of the nerve and vessel alignment in the whisker follicle, we performed whole-mount follicle staining with anti-neurofilament and VE-cadherin antibodies. The blood vessel layer is separated from the trigeminal nerve layer along with whole follicle shaft (Figure 6G). However, the nerve and vessel alignment is overlapped in multiple regions in the whole follicle shaft (Figure 6H). Therefore, Sema3E-Plexin-D1 signaling is required in vivo for proper nerve and vessel organization in the whisker follicle.

Attractive Signals for the Initial Recruitment of Nerve and Vessel Are Expressed in the Whisker Follicles

Our data demonstrated that, in the developing whisker pad, the nerve and vessel are initially intermingled, then the nerve ring forms, followed by the vessel ring, to eventually establish the double ring structure with the nerve ring inside and vessel ring outside. Moreover, the nerve and vessel rings are formed independently of each other, rather than "one patterning the other." Sema3E originating from the mesenchymal sheath surrounding the hair follicles controls their relative position in the double ring structure through its receptor Plexin-D1. What are the signals that initially recruit nerves and vessels in the whisker follicle? Two major chemoattractants for nerve and vessel recruitment, nerve growth factor (NGF) and VEGF, respectively, are expressed around the whisker follicle when the double ring structure is forming (Bandtlow et al., 1987; Genç et al., 2005) (Figure S5). At E12.5, when the nerve ring begins to form, we detected TrkA (NGF receptor) expression in the trigeminal nerves and *Ngf* expression around each whisker primordium (Figures S5A–S5H). Moreover, TG and maxillary explant coculture assay demonstrated that NGF is necessary to attract TG axons (O'Connor and Tessier-Lavigne, 1999), suggesting that NGF-TrkA signaling contributes to the initial nerve ring formation. To directly test this hypothesis, we analyzed the initial nerve ring formation in mice lacking *Ngf* at E12.5–E13.5. We observed a normal size of TG and normal peripheral projections of trigeminal nerves to the snout area in *Ngf* mutant mice, consistent with the previous finding that mouse TG survival becomes NGF dependent after E14.5 (Figures S6A and S6B) (Piñon et al., 1996). However, despite normal arrival at the whisker pad, TG axons failed to form the initial ring-like structure in the *Ngf* mutant embryos. At E12.5, when a ring-like structure of axonal innervation forms

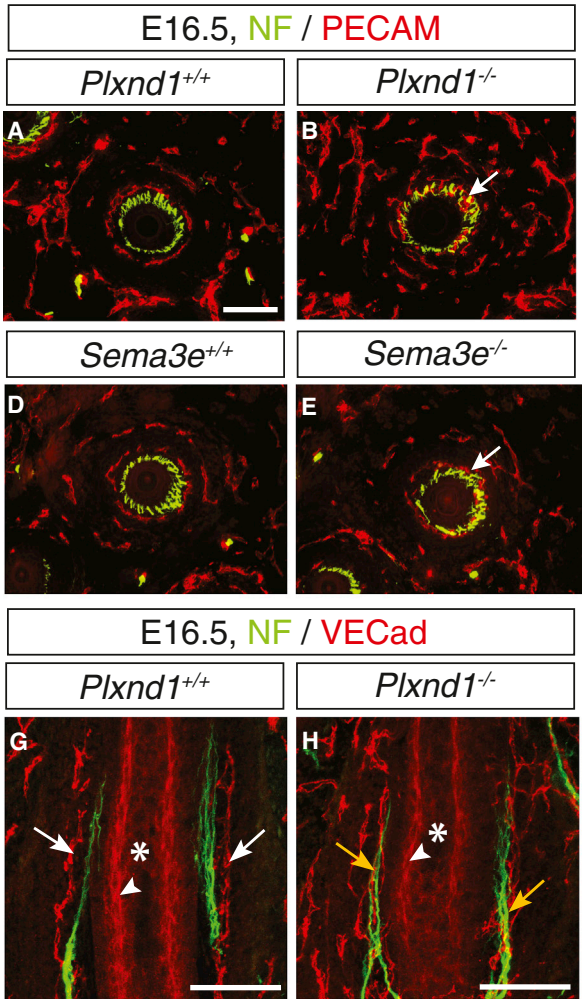

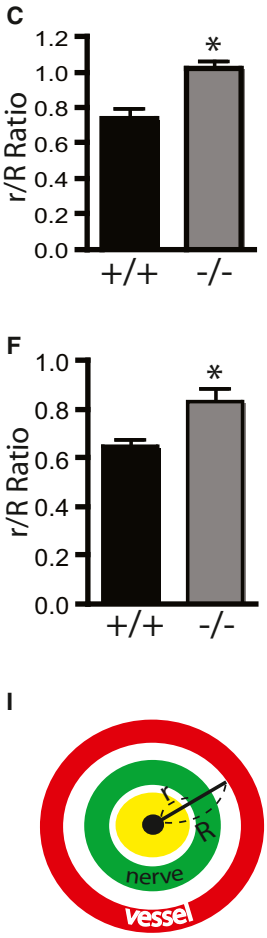

Figure 6. Plexin-D1 and Sema3E Is Required for the Stereotypic Double Ring Nerve/Vessel Patterning in the Whisker Pad In Vivo

(A–C) *Plxnd1* null mice exhibit severe nerve/vessel organization defects. The whisker follicle region of *Plxnd1* mutants (B) and their littermate controls (A) at E16.5 were sectioned and immunostained with neurofilament (NF) and PECAM. In the *Plxnd1* mutant, nerve and vessel rings were abnormally close, with some areas showing complete vessel/nerve intermingling, indicated by an arrow in (B). Radii of the vessel ring (R) and nerve ring (r) depicted in (I) were measured, and their ratio was calculated for each follicle (C). *Sema3e* null mice also show the same nerve/vessel patterning phenotype, indicated by the white arrow in (E), compared to their littermate controls (D), and r/R ratio measurement is shown in (F). For the quantification, six to eight whisker follicles per animal from three different pairs of embryos in each experimental condition were measured, and the mean ratios ± SEM are shown in (C) and (F). Paired Student's t test; *$p < 0.05$. The detail patterning phenotype was analyzed in coronal view of whisker follicles using confocal imaging process after neurofilament and VE-cadherin whole-mount staining. The blood vessel layer, indicated by white arrows in (G), is clearly separated from the TG nerve layer in wild-type (G); but in the *Plxnd1* mutant, vessels, indicated by yellow arrows in (H), are intermingled with nerve layers (H). White arrowheads in (G) and (H) indicate nonspecific signals from the whisker sheath marked in white asterisks. Scale bars, 100 μm in (A), (B), (D), and (E) and 50 μm in (G) and (H).
See also Figure S4.

around each whisker primordium in the wild-type littermates (Figures 1C, S6C–S6D, and S6G), the axonal innervation in *Ngf* mutant embryos aggregates and fails to form the fasciculated ring-like structure (Figures S6E–S6G). At E13.5, when a complete nerve ring structure forms in the wild-type littermates (Figure S6H), the axonal innervation still "wanders" and fails to form a ring structure around the whisker primordium (Figure S6I). In addition, this initial failure of nerve ring formation defect seems to be continued postnatally, because whisker innervation defects have also been observed in newborn *Bax*$^{-/-}$*; TrkA*$^{-/-}$ mice (Patel et al., 2000). Together, these data provide in vivo evidence demonstrating that NGF signaling is critical for the initial nerve ring formation. At E13.5, right before the blood vessel ring forms, we detected strong VEGF expression around each whisker primordium in an area close to the nerve ring (Figures S5I–S5K). Moreover, endothelial-specific knockout of *Npn1*, a VEGF receptor, results in aberrant vessel ring formation (Figures 2E and 2F). These data demonstrate that VEGF signaling contributes to the initial vessel ring formation. Interestingly, both NGF- and VEGF-expressing cells are arrayed along the circumference of the primordium, thereby enabling the recruitment of both nerve and vessel in a ring-like structure during development. At E14.5, the repulsive signaling of Sema3E-Plexin-D1 emerges to set the two rings apart and achieve the double ring structure. Thus, these results suggest that balanced attractive and repulsive signals from the target tissue control the ontogenetic patterning of the neurovascular double ring structure (Figure 7).

Taken together, the findings in this study demonstrate that the stereotypic neurovascular congruency in complex tissue is established during development by an independent patterning mechanism by cues that emanated from the target tissue. Using the mouse whisker pad as a model system, we found that nerves and vessels form a stereotypic double ring neurovascular structure around each of the whisker follicles during development. It is surprising that this double ring neurovascular congruency is not established by a "one-patterns-the-other" mechanism but rather is established via a mechanism in which nerves and vessels are patterned independently through differential responses to a common guidance cue. Sema3E secreted from the center of the follicle has the potential to repel both nerves and vessels through Plexin-D1. However, differential Plexin-D1 expression in nerves and vessels during whisker follicle development is translated into a distinctive repulsive strength that defines the relative location of nerve and vessel rings. Finally, formation of

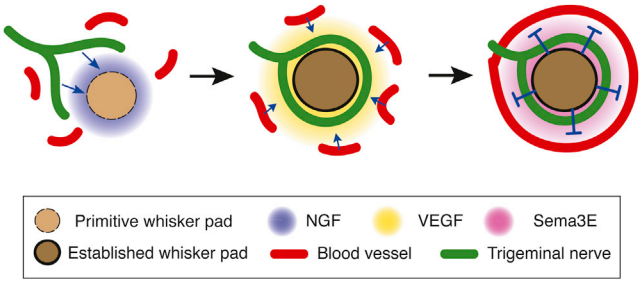

Figure 7. Model of How Stereotypic Double Ring Neurovascular Structure Is Established during Development

Left: during early development (E11–E12), NGF is expressed in tissue surrounding the primitive whisker follicle and attracts trigeminal axons to the whisker target area. At this stage, the blood vessel plexus is dispersed in the whisker follicle and is not organized. Middle: As development progress, around E13–E14 when the trigeminal nerve forms a nerve ring structure, VEGF expression in the whisker follicle region begins to recruit blood vessel close to the nerve ring. Right: around E14–E16, Sema3E starts to be expressed in the mesenchymal sheath of the whisker follicle and repels incoming vessels through its interaction with Plexin-D1, which then settle outside of the nerve ring. Although Plexin-D1 is also expressed in the trigeminal nerve at this stage, its expression in the axon terminals is selectively downregulated to a level that is not sufficient to respond to Sema3E, thereby maintaining the location of the nerve ring close to the whisker follicle.
See also Figures S5 and S6.

this double ring structure is disrupted in mice lacking *Plxnd1* and *Sema3e*. Unlike the previously described "one-patterns-the-other" mechanism (Mukouyama et al., 2002), our study demonstrates that local signals act as a central organizer in complex tissues to establish neurovascular congruency via an independent patterning mechanism.

DISCUSSION

In this study, we address a critical developmental question about which little is known—how nerves and blood vessels form congruent patterns to facilitate their interdependent functions. We demonstrate that neurovascular congruency in the whisker follicle is not established by a "one-patterns-the-other" mechanism but rather patterned independently through a balance of attractive and repulsive cues originating from the surrounding environment to achieve the final congruent double ring structure.

While NGF and VEGF can serve as the initial attractive cues to organize nerves and vessels, respectively, to the center around the hair follicle, Sema3E is responsible for positioning the two rings to the final double ring structure with the nerve ring inside and vessel ring outside. Even though Sema3E-Plexin-D1 signaling exerts repulsive signals in both neurons and endothelial cells (Figure 4) (Oh and Gu, 2013; Ding et al., 2012), the nerve ring and vessel ring respond differently to this repulsive signal because of different levels of Plexin-D1 in the nerve and vessel rings. In the case of vessels, Plexin-D1 level is high and, therefore, vessels actively respond to Sema3E's repulsive signal, resulting in the outer ring position. In contrast, the selective downregulation of Plexin-D1 protein levels in the nerve terminal removes the sensitivity of the axons to the repulsive ligand, resulting in the inner nerve ring position, thereby allowing the whole final double ring structure to form. What is the potential mechanism underlying the selective Plexin-D1 protein downregulation at the nerve terminal? Recently, a study of the mouse spinal cord demonstrated that calpain-mediated proteolytic processing of the Plexin A1 receptor in precrossing commissural axons prevents responsiveness to the repulsive cue Sema3B, until the axons have crossed the midline (Nawabi et al., 2010). Indeed protease-mediated regulation of receptor levels plays a critical role in controlling spatial and temporal aspects of ligand responsiveness during neural development and disease (Bai and Pfaff, 2011). We postulate that a similar mechanism of protease activity might be responsible for the selective downregulation of Plexin-D1 at the nerve terminal to silence the nerve ring responsiveness to Sema3E. Another possibility is that the selective downregulation of Plexin-D1 happens at the local translation level. Recent studies demonstrated that the local synthesis of axon guidance receptors can be controlled at the translational level (Colak et al., 2013; Tcherkezian et al., 2010). Testing these hypotheses will be of interest in future studies.

The use of an independent patterning mechanism in establishing neurovascular congruency provides an intriguing contrast with the "one-patterns-the-other" model shown in previous studies of the limb skin and sympathetic system. In the developing mouse forelimb skin, peripheral sensory nerves determine the differentiation and branching pattern of arteries (Mukouyama et al., 2002, 2005; Li et al., 2013), indicating that the nerve guides the vessel. Conversely, there are also cases where vessels can express signals that then attract axons. For example, artemin is expressed in the smooth muscle cells of the vessels and attracts sympathetic fibers to follow these blood vessels (Honma et al., 2002). Similarly, blood-vessel-expressed endothelins direct the extension of sympathetic axons from the superior cervical ganglion to the external carotid artery (Makita et al., 2008). This "one-patterns-the-other" mechanism was thought to represent a general rule governing the establishment of neurovascular congruency. However, in these examples, there is a relatively simple organization of the aligned nerves and vessels, and neurovascular networks in different tissues are very diverse. Here, in the whisker pad, the double ring neurovascular congruency is not established by one system patterning the other but rather by an independent patterning mechanism.

Why should two distinct mechanisms be used to establish congruency? In the case of a target tissue with a planar structure or during pathfinding before reaching a target, the "one-patterns-the-other" model allows for the parallel trajectories of nerves and vessels, independent of their position relative to their surroundings. However, in target tissues with complex 3D structures, the precise architecture of the trio of nerves, vessels, and target tissues becomes functionally relevant. This functional organization is clearly the case in the whisker follicles, where the nerve ring must be located closer to, and the vessel ring farther from, the whisker pad to enable proper neurovascular regulation of the whisker itself. The independent or coordinate patterning model enables the target tissue to act as a central organizer to control the coordinated development of multiple tissue subcomponents. Given the diversity of neurovascular structures in various tissues and the variable timing of neural innervation and vascular ingression in various tissues, local

signals provided by a central organizer within the specific target tissue may be a common mechanism used to establish neurovascular congruency patterns that facilitate target tissue function.

The close anatomic apposition between nerves and vessels is critical for their functional interdependence, and revealing the signals that mediate the tight neurovascular association provides insights into our understanding of nervous system function. This is more evident in the brain where neural cells (neurons and glia) and vascular cells (endothelia and pericytes) form a functionally integrated network that is collectively termed the neurovascular unit (Iadecola, 2004). Neurovascular unit integrity has recently been shown to regulate important physiological functions and is linked to the onset and progression of various neurodegenerative diseases. For example, a deficient endothelial-secreted PDGF-BB-PDGFβ signaling on pericytes within the vascular system leads to defects in cerebrovascular integrity and, subsequently, results in neuronal dysfunction (Armulik et al., 2010; Bell et al., 2010; Daneman et al., 2010). Similarly, a recent study shows that deficient signaling between astrocyte-secreted apoE, a major risk factor for Alzheimer's disease, and its binding protein LRP1 on pericytes can also lead to cerebrovascular defects followed by neuronal degeneration (Bell et al., 2012). The functional consequences of periphery neurovascular congruency defects on nervous system function are less understood. In the whisker system, earlier studies suggest that the vascular component affiliated with each whisker both affects the movement of the whisker and modulates the sensitivity of the sensory nerve endings (Fundin et al., 1997; Wineski, 1985). It will be an important future direction to use the animal model we have generated here to investigate whether developmental deficits in establishing neurovascular patterning in the whisker pad target areas will manifest as functional and behavioral deficits in the mature animals. Both the peripheral TG and higher level barrel cortical electrophysiological properties in response to whiskering can be used as neural functional readouts. It will also be interesting to examine functional consequence of neurovascular congruency defects in other peripheral examples such as forelimb skin sensory axon/arterial branching system (Mukouyama et al., 2002, 2005; Li et al., 2013) and the mouse sympathetic axon/blood vessel (Honma et al., 2002; Makita et al., 2008). Understanding how highly stereotyped neurovascular structure is formed to facilitate organ-specific functions will provide insights into the homeostasis and pathogenesis of medical disorders that involve both nerves and vessels.

EXPERIMENTAL PROCEDURES

Animals

Plxnd1$^{flox/flox}$ mice (Kim et al., 2011), *Nestin-Cre* mice (Tronche et al., 1999), and *Tie2-Cre* mice (Kisanuki et al., 2001) were maintained on a C57Bl/6 background. *Plxnd1*$^{+/-}$ mice (Gu et al., 2005), *Npn1* mice (Gu et al., 2003), and *Vegf*^{lacZ} mice (Miquerol et al., 1999) were maintained on an outbred Swiss Webster background. *Sema3e*$^{+/-}$ mice were maintained on an 129SVE background. *Ngn1* (Ma et al., 1998) and *Ngf* (Crowley et al., 1994) knockout embryos were obtained from Dr. Quifu Ma (Harvard Medical School) and Dr. Rejji Kuruvilla (Johns Hopkins University), respectively. Swiss Webster, C57Bl/6, and 129SVE wild-type mice were obtained from Taconic Farms. All animals were treated according to institutional and National Institutes of Health guidelines approved by the Institutional Animal Care and Use Committee at Harvard Medical School.

Immunohistochemistry

Embryos were removed, immediately frozen in liquid nitrogen, and sectioned at 16 μm using a cryostat (Leica). Sections were fixed in 4% paraformaldehyde (PFA) for 5 min and briefly washed in 1× PBS several times at room temperature. After washing, sections were blocked in 1× PBS containing 0.1% Triton X-100 (PBST) and 10% normal goat serum for 1 hr and then incubated with primary antibodies in blocking buffer at 4°C overnight. For Plexin-D1 immunohistochemisty, embryos were fixed in 4% PFA in 0.1 M phosphate buffer (pH 7.5) for 2 hr and equilibrated in 30% sucrose at 4°C overnight. The antibodies used are: α-neurofilament (1:100; Item No. 2H3, Developmental Studies Hybridoma Bank), α-PECAM (1:500; 553370, BD Pharmingen), α-Plexin-D1 (1:6,000, a gift from Dr. Yutaka Yoshida, Cincinnati Children's Hospital), and α-TrkA (1:500; 06-574, Millipore). After washing in 1× PBST for 5 min three times, sections were incubated in Alexa Fluor-conjugated secondary antibodies (1:1,000, Invitrogen) for 1 hr, then washed several times in PBST, and mounted with Fluoromount G (Electron Microscopy Sciences). Immunostained sections were analyzed by fluorescence microscopy using a Nikon Eclipse 80i microscope equipped with a Nikon DS-2 digital camera. Images were processed using Adobe Photoshop and ImageJ (National Institutes of Health).

Whole-Mount Immunostaining

For whole-mount whisker follicle staining, embryos were fixed in 4% PFA for 6 hr and equilibrated in 30% sucrose at 4°C overnight. Embryo snout areas were sectioned at 100 μm using a cryostat (Leica) and blocked in 1× PBST, 10% DMSO, and 5% normal goat serum for 1 hr, and then incubated with primary antibodies in blocking buffer at room temperature for 2 days. The antibodies used were α-neurofilament (1:50; 2H3) and α-VE-cadherin (1:100; ab33168, Abcam). After washing in 1× PBST for 1 hr five times, sections were incubated in Alexa Fluor-conjugated secondary antibodies (1:500, Invitrogen), diluted in the blocking buffer for 1 day, then washed several times in PBST, and dehydrated with 100% methanol. Before mounting, sections were cleared with benzyl alcohol and benzyl benzoate mixture. Sections were analyzed by confocal laser-scanning microscopy using a Zeiss LSM 510 META confocal microscope.

In Situ Hybridization

Nonradioactive ISH for tissue sections and whole-mount ISH were performed according to standard methods (Gu et al., 2005). Briefly, 16-μm-thick cryosections were fixed in 4% PFA, acetylated in 1% triethanolamine and 0.25% acetic anhydride, prehybridized, and hybridized with indicated probes at 60°C. After hybridization, sections were washed and incubated with sheep anti-Digoxigenin-AP antibody (1:3,000, Roche) for 90 min at room temperature. After several washes, sections were incubated in BM Purple (Roche) until positive signal was detected. To perform immunostaining on the same section after ISH, sections were washed in 1× PBS several times and postfixed in 4% PFA for 5 min. After fixation, all procedures were followed as described earlier in the immunohistochemistry section.

Double fluorescence ISH was performed using the tyramide signal amplification method according to the manufacturer's instructions (NEL753001KT, PerkinElmer). Two fluorescein isothiocyanate- or Digoxigenin-labeled antisense probes were simultaneously hybridized and stained by fluorescein or Cy3 chromogens, respectively.

The following antisense probes were used: *Plxnd1* (Kim et al., 2011), *Sema3e* (Gu et al., 2005), *Npn1* (He and Tessier-Lavigne, 1997), and *Flk-1* (NM_010612, nt1277-2249).

Ligand Preparation and AP-Ligand Binding Assay

AP-tagged ligands were produced in HEK293T cells as described elsewhere (Gu et al., 2002). Expression construct was transfected into cells by LipofectAMINE 2000 (Invitrogen), and conditioned medium was harvested at 48 hr posttransfection. For AP-ligand binding assay (Gu et al., 2003), 20-μm-thick cryosections were fixed in cold methanol and preincubated in 1× PBS containing 4 mM $MgCl_2$ and 10% fetal bovine serum for 1 hr. Sections were incubated in the binding solution (1× PBS-$MgCl_2$ plus 20 mM HEPES,

pH 7.0) containing 1–2 nM ligands for 2 hr at room temperature. After several washes in 1× PBS-$MgCl_2$, sections were fixed in acetone and formaldehyde fixative and then heat inactivated at 65°C for 2 hr. For AP chromogenic development, sections were incubated in AP buffer (100 mM Tris-HCl, pH 9.5, 100 mM NaCl, 5 mM $MgCl_2$) containing 4-Nitro blue tetrazolium chloride and 5-Bromo-4-chloro-3-indolyl-phosphate (Roche).

Growth Cone Collapse Assay

TG explant growth cone collapse assay was performed as described elsewhere (Behar et al., 1999). Briefly, TG explants isolated from E14.5 embryos are placed on growth-factor-reduced Matrigel (356230, BD)-coated cover glasses and cultured overnight at 37°C in DMEM/F12 containing 0.6 mg/ml cellulose and 20 ng/ml NGF (a gift from Dr. Rejji Kuruvilla, Johns Hopkins University). The next day, without removing culture media, 2× concentrated prewarmed ligands (Kim et al., 2011) were applied to explants for 30 min and immediately fixed in 4% PFA for 30 min. After three washes in 1× PBS and blocking, explants were incubated with anti-neurofilament antibody (1:100), followed by anti-mouse Alexa 488-conjugated secondary antibody (1:1,000) and Alexa 568-conjugated phalloidin (1:50) mixture incubation. Then explants were washed in 1× PBS several times and mounted blindly. To quantify collapsed growth cone, randomly selected fields of TG neurons were imaged and collapsed versus intact growth cones were scored as done in previous reports (Cox et al., 1990; Ughrin et al., 2003). Briefly, growth cones with broad lamellipodia were defined as intact, whereas growth cones lacking lamellipodia and having only a few sharp filopodia were counted as collapsed.

HUVEC Migration Assay

HUVECs (CC-2517, Lonza) were maintained in EBM-2 basal medium (CC-3156, Lonza) supplemented with EGM-2 growth factor mixture (CC-4176, Lonza). HUVECs (5×10^4) were seeded on the upper chamber of a fibronectin (Calbiochem)-coated Transwell insert (Falcon 3097, 8 μm pore size) with 0.5 nM ligands with or without 50 ng/ml of VEGF in the lower chamber. After 5 hr incubation, filters were fixed in 4% PFA and stained with 0.5% crystal violet for 10 min. Migrated HUVECs were imaged, and random fields from each image were counted to calculate the migrated cell number per area.

Statistical Analysis

Statistical analyses were performed using Prism4 (GraphPad Software). Summary data are reported as mean ± SD or mean ± SEM. Multiple samples were analyzed with a one-way ANOVA, and two samples were analyzed with a nonparametric Student's t test. $p < 0.05$ was considered as statistically significant.

SUPPLEMENTAL INFORMATION

Supplemental Information includes Supplemental Experimental Procedures, six figures, and three movies and can be found with this article online at http://dx.doi.org/10.1016/j.neuron.2013.09.005.

ACKNOWLEDGMENTS

We thank Drs. Bob Datta, Michael Greenberg, Rejji Kuruvilla, Qiufu Ma, Alex Kolodkin, and members of the C.G. laboratory for helpful comments on the manuscript; Dr. Qiufu Ma for providing *Ngn1* knockout embryos; Drs. Rejji Kuruvilla and Rajshri Joshi for providing NGF and *Ngf* knockout embryos; Dr. David Ginty and Siyi Huang for providing *Ngf* knockout embryos; Dr. Yutaka Yoshida for providing *Plxnd1*$^{flox/flox}$ mice and anti-Plexin-D1 antibody; Drs. Christopher Henderson and Fanny Mann for providing *Sema3e* mice; Dr. Susan Dymecki for providing *Nestin-Cre* mice and *Vegf-lacZ* mice; Dr. Reha Erzurumlu for technical advice; the National Cancer Institute-Frederick for providing VEGF; and the Optical Imaging Program at the Harvard NeuroDiscovery Center for helping with confocal images. This work was supported by a Lefler postdoctoral fellowship (W.O.), an Alice and Joseph Brooks Fund Postdoctoral Fellowship (W.O.), and the following grants to C.G.: a Sloan Research Fellowship, a March of Dimes Basil O'Connor award, an Armenise Junior Faculty award, and National Institutes of Health Grant R01NS064583.

Accepted: August 29, 2013
Published: October 16, 2013

REFERENCES

Adams, R.H., and Eichmann, A. (2010). Axon guidance molecules in vascular patterning. Cold Spring Harb. Perspect. Biol. *2*, a001875.

Armulik, A., Genové, G., Mäe, M., Nisancioglu, M.H., Wallgard, E., Niaudet, C., He, L., Norlin, J., Lindblom, P., Strittmatter, K., et al. (2010). Pericytes regulate the blood-brain barrier. Nature *468*, 557–561.

Bai, G., and Pfaff, S.L. (2011). Protease regulation: the Yin and Yang of neural development and disease. Neuron *72*, 9–21.

Bandtlow, C.E., Heumann, R., Schwab, M.E., and Thoenen, H. (1987). Cellular localization of nerve growth factor synthesis by in situ hybridization. EMBO J. *6*, 891–899.

Bates, D., Taylor, G.I., Minichiello, J., Farlie, P., Cichowitz, A., Watson, N., Klagsbrun, M., Mamluk, R., and Newgreen, D.F. (2003). Neurovascular congruence results from a shared patterning mechanism that utilizes Semaphorin3A and Neuropilin-1. Dev. Biol. *255*, 77–98.

Behar, O., Mizuno, K., Badminton, M., and Woolf, C.J. (1999). Semaphorin 3A growth cone collapse requires a sequence homologous to tarantula hanatoxin. Proc. Natl. Acad. Sci. USA *96*, 13501–13505.

Bell, R.D., Winkler, E.A., Sagare, A.P., Singh, I., LaRue, B., Deane, R., and Zlokovic, B.V. (2010). Pericytes control key neurovascular functions and neuronal phenotype in the adult brain and during brain aging. Neuron *68*, 409–427.

Bell, R.D., Winkler, E.A., Singh, I., Sagare, A.P., Deane, R., Wu, Z., Holtzman, D.M., Betsholtz, C., Armulik, A., Sallstrom, J., et al. (2012). Apolipoprotein E controls cerebrovascular integrity via cyclophilin A. Nature *485*, 512–516.

Bellon, A., Luchino, J., Haigh, K., Rougon, G., Haigh, J., Chauvet, S., and Mann, F. (2010). VEGFR2 (KDR/Flk1) signaling mediates axon growth in response to semaphorin 3E in the developing brain. Neuron *66*, 205–219.

Carmeliet, P., and Tessier-Lavigne, M. (2005). Common mechanisms of nerve and blood vessel wiring. Nature *436*, 193–200.

Chauvet, S., Cohen, S., Yoshida, Y., Fekrane, L., Livet, J., Gayet, O., Segu, L., Buhot, M.C., Jessell, T.M., Henderson, C.E., and Mann, F. (2007). Gating of Sema3E/PlexinD1 signaling by neuropilin-1 switches axonal repulsion to attraction during brain development. Neuron *56*, 807–822.

Colak, D., Ji, S.J., Porse, B.T., and Jaffrey, S.R. (2013). Regulation of axon guidance by compartmentalized nonsense-mediated mRNA decay. Cell *153*, 1252–1265.

Cox, E.C., Müller, B., and Bonhoeffer, F. (1990). Axonal guidance in the chick visual system: posterior tectal membranes induce collapse of growth cones from the temporal retina. Neuron *4*, 31–37.

Crowley, C., Spencer, S.D., Nishimura, M.C., Chen, K.S., Pitts-Meek, S., Armanini, M.P., Ling, L.H., McMahon, S.B., Shelton, D.L., Levinson, A.D., et al. (1994). Mice lacking nerve growth factor display perinatal loss of sensory and sympathetic neurons yet develop basal forebrain cholinergic neurons. Cell *76*, 1001–1011.

Daneman, R., Zhou, L., Kebede, A.A., and Barres, B.A. (2010). Pericytes are required for blood-brain barrier integrity during embryogenesis. Nature *468*, 562–566.

Ding, J.B., Oh, W.J., Sabatini, B.L., and Gu, C. (2012). Semaphorin 3E-Plexin-D1 signaling controls pathway-specific synapse formation in the striatum. Nat. Neurosci. *15*, 215–223.

Ebara, S., Kumamoto, K., Matsuura, T., Mazurkiewicz, J.E., and Rice, F.L. (2002). Similarities and differences in the innervation of mystacial vibrissal follicle-sinus complexes in the rat and cat: a confocal microscopic study. J. Comp. Neurol. *449*, 103–119.

Erzurumlu, R.S., Murakami, Y., and Rijli, F.M. (2010). Mapping the face in the somatosensory brainstem. Nat. Rev. Neurosci. *11*, 252–263.

Fundin, B.T., Pfaller, K., and Rice, F.L. (1997). Different distributions of the sensory and autonomic innervation among the microvasculature of the rat mystacial pad. J. Comp. Neurol. *389*, 545–568.

Gelfand, M.V., Hong, S., and Gu, C. (2009). Guidance from above: common cues direct distinct signaling outcomes in vascular and neural patterning. Trends Cell Biol. *19*, 99–110.

Genç, B., Ulupinar, E., and Erzurumlu, R.S. (2005). Differential Trk expression in explant and dissociated trigeminal ganglion cell cultures. J. Neurobiol. *64*, 145–156.

Gu, C., Limberg, B.J., Whitaker, G.B., Perman, B., Leahy, D.J., Rosenbaum, J.S., Ginty, D.D., and Kolodkin, A.L. (2002). Characterization of neuropilin-1 structural features that confer binding to semaphorin 3A and vascular endothelial growth factor 165. J. Biol. Chem. *277*, 18069–18076.

Gu, C., Rodriguez, E.R., Reimert, D.V., Shu, T., Fritzsch, B., Richards, L.J., Kolodkin, A.L., and Ginty, D.D. (2003). Neuropilin-1 conveys semaphorin and VEGF signaling during neural and cardiovascular development. Dev. Cell *5*, 45–57.

Gu, C., Yoshida, Y., Livet, J., Reimert, D.V., Mann, F., Merte, J., Henderson, C.E., Jessell, T.M., Kolodkin, A.L., and Ginty, D.D. (2005). Semaphorin 3E and plexin-D1 control vascular pattern independently of neuropilins. Science *307*, 265–268.

He, Z., and Tessier-Lavigne, M. (1997). Neuropilin is a receptor for the axonal chemorepellent Semaphorin III. Cell *90*, 739–751.

Honma, Y., Araki, T., Gianino, S., Bruce, A., Heuckeroth, R., Johnson, E., and Milbrandt, J. (2002). Artemin is a vascular-derived neurotropic factor for developing sympathetic neurons. Neuron *35*, 267–282.

Iadecola, C. (2004). Neurovascular regulation in the normal brain and in Alzheimer's disease. Nat. Rev. Neurosci. *5*, 347–360.

Katsume, Y., Yoshizuka, M., Annoura, S., Miyazaki, M., and Fujimoto, S. (1984). Interendothelial cytoplasmic bridge of blood sinus in rabbit sinus hair. J. Electron Microsc. (Tokyo) *33*, 175–177.

Kim, J., Oh, W.J., Gaiano, N., Yoshida, Y., and Gu, C. (2011). Semaphorin 3E-Plexin-D1 signaling regulates VEGF function in developmental angiogenesis via a feedback mechanism. Genes Dev. *25*, 1399–1411.

Kisanuki, Y.Y., Hammer, R.E., Miyazaki, J., Williams, S.C., Richardson, J.A., and Yanagisawa, M. (2001). Tie2-Cre transgenic mice: a new model for endothelial cell-lineage analysis in vivo. Dev. Biol. *230*, 230–242.

Kobayashi, H., Koppel, A.M., Luo, Y., and Raper, J.A. (1997). A role for collapsin-1 in olfactory and cranial sensory axon guidance. J. Neurosci. *17*, 8339–8352.

Lewis, W. (1902). The development of the arm in man. Am. J. Anat. *1*, 145–185.

Li, W., Kohara, H., Uchida, Y., James, J.M., Soneji, K., Cronshaw, D.G., Zou, Y.R., Nagasawa, T., and Mukouyama, Y.S. (2013). Peripheral nerve-derived CXCL12 and VEGF-A regulate the patterning of arterial vessel branching in developing limb skin. Dev. Cell *24*, 359–371.

Ma, Q., Chen, Z., del Barco Barrantes, I., de la Pompa, J.L., and Anderson, D.J. (1998). neurogenin1 is essential for the determination of neuronal precursors for proximal cranial sensory ganglia. Neuron *20*, 469–482.

Makita, T., Sucov, H.M., Gariepy, C.E., Yanagisawa, M., and Ginty, D.D. (2008). Endothelins are vascular-derived axonal guidance cues for developing sympathetic neurons. Nature *452*, 759–763.

Martin, P., and Lewis, J. (1989). Origins of the neurovascular bundle: interactions between developing nerves and blood vessels in embryonic chick skin. Int. J. Dev. Biol. *33*, 379–387.

Miquerol, L., Gertsenstein, M., Harpal, K., Rossant, J., and Nagy, A. (1999). Multiple developmental roles of VEGF suggested by a LacZ-tagged allele. Dev. Biol. *212*, 307–322.

Mukouyama, Y.S., Shin, D., Britsch, S., Taniguchi, M., and Anderson, D.J. (2002). Sensory nerves determine the pattern of arterial differentiation and blood vessel branching in the skin. Cell *109*, 693–705.

Mukouyama, Y.S., Gerber, H.P., Ferrara, N., Gu, C., and Anderson, D.J. (2005). Peripheral nerve-derived VEGF promotes arterial differentiation via neuropilin 1-mediated positive feedback. Development *132*, 941–952.

Nawabi, H., Briançon-Marjollet, A., Clark, C., Sanyas, I., Takamatsu, H., Okuno, T., Kumanogoh, A., Bozon, M., Takeshima, K., Yoshida, Y., et al. (2010). A midline switch of receptor processing regulates commissural axon guidance in vertebrates. Genes Dev. *24*, 396–410.

O'Connor, R., and Tessier-Lavigne, M. (1999). Identification of maxillary factor, a maxillary process-derived chemoattractant for developing trigeminal sensory axons. Neuron *24*, 165–178.

Oh, W.J., and Gu, C. (2013). The role and mechanism-of-action of Sema3E and Plexin-D1 in vascular and neural development. Semin. Cell Dev. Biol. *24*, 156–162.

Patel, T.D., Jackman, A., Rice, F.L., Kucera, J., and Snider, W.D. (2000). Development of sensory neurons in the absence of NGF/TrkA signaling in vivo. Neuron *25*, 345–357.

Piñon, L.G., Minichiello, L., Klein, R., and Davies, A.M. (1996). Timing of neuronal death in trkA, trkB and trkC mutant embryos reveals developmental changes in sensory neuron dependence on Trk signalling. Development *122*, 3255–3261.

Quaegebeur, A., Lange, C., and Carmeliet, P. (2011). The neurovascular link in health and disease: molecular mechanisms and therapeutic implications. Neuron *71*, 406–424.

Stainier, D.Y., and Gilbert, W. (1990). Pioneer neurons in the mouse trigeminal sensory system. Proc. Natl. Acad. Sci. USA *87*, 923–927.

Taylor, G.I., Gianoutsos, M.P., and Morris, S.F. (1994). The neurovascular territories of the skin and muscles: anatomic study and clinical implications. Plast. Reconstr. Surg. *94*, 1–36.

Tcherkezian, J., Brittis, P.A., Thomas, F., Roux, P.P., and Flanagan, J.G. (2010). Transmembrane receptor DCC associates with protein synthesis machinery and regulates translation. Cell *141*, 632–644.

Tronche, F., Kellendonk, C., Kretz, O., Gass, P., Anlag, K., Orban, P.C., Bock, R., Klein, R., and Schütz, G. (1999). Disruption of the glucocorticoid receptor gene in the nervous system results in reduced anxiety. Nat. Genet. *23*, 99–103.

Ughrin, Y.M., Chen, Z.J., and Levine, J.M. (2003). Multiple regions of the NG2 proteoglycan inhibit neurite growth and induce growth cone collapse. J. Neurosci. *23*, 175–186.

van der Zwaag, B., Hellemons, A.J., Leenders, W.P., Burbach, J.P., Brunner, H.G., Padberg, G.W., and Van Bokhoven, H. (2002). PLEXIN-D1, a novel plexin family member, is expressed in vascular endothelium and the central nervous system during mouse embryogenesis. Dev. Dyn. *225*, 336–343.

Wineski, L.E. (1985). Facial morphology and vibrissal movement in the golden hamster. J. Morphol. *183*, 199–217.

Zlokovic, B.V. (2008). The blood-brain barrier in health and chronic neurodegenerative disorders. Neuron *57*, 178–201.

Zlokovic, B.V. (2011). Neurovascular pathways to neurodegeneration in Alzheimer's disease and other disorders. Nat. Rev. Neurosci. *12*, 723–738.